Response to reviewer

Dear Dr. Kaiser,

Thank you for reviewing the revised manuscript and checking the deposited data. We have changed the ppb into nmol mol^{-1} in the data table. Sorry for this mistake and thank you for pointing it out. Also, during last revision, we also revised the file on Open Science Framework (on June 24, same time as we upload the last draft) to make it as the same format as Table 1, so it might take a while for the system to process the file.

Additionally, we would like to thank Ms. Anna Wenzel, editorial support at ACP, for kindly helping us removing the latest supplementary material during the last revision. However, it seems that the old versions of the supplementary material were still in the systems. Therefore, in this round you might again see a supplementary file (which was an older version). Since we are not able to delete it from our end, please ignore the file, and if it causes further problem or confusion, we will contact the editorial office to remove it again.

Here is our response to your comment about the EIE calculation:

For the regression of our EIE calculation, we agree that an unforced linear regression for the five dark experiments will yield a slope of 33.9‰ instead of our proposed 28.1‰. It would also be nice if our results can show a good consensus with previous studies, especially from our own lab. However, we think it is probably not the case here.

This unforced regression yields an intercept of -2.5‰, which do not agree with the mathematical equation (Eq. 3). Theoretically, when $f(NO_2)=1$, the $\delta^{15}N$ value of NO_2 should be equal to NO_x (because all NO_x is in the form of NO_2), therefore the $(\delta(NO_2)-\delta(NO_x))/(1+\delta(NO_2))$ value should be 0. Referee 2 suggested that this -2.5‰ intercept might represent a systematic error (^{17}O interference) when measuring the $\delta^{15}N$ values on the IRMS: when there is oxygen isotope mass independent fractionation, measuring the $\delta^{15}N$ will have a systematic error (approximately -1.5‰ when ^{17}O excess is 30‰). This error will become a problem if one used NO_x gas with known $\delta(NO_x)$ value, then measure the $\delta(NO_2)$, in this case the intercept of the graph would not be 0. However, in our calculations, the $\delta(NO_x)$ values were also measured by the same method as $\delta(NO_2)$, it should have the same systematic error. As a result, **subtracting $\delta(NO_2)$ with $\delta(NO_x)$ should cancel out this systematic error**. Therefore, the intercept of this linear regression should be 0.

The above argument can be validated if we incorporate the data from "determining $\delta(NO_x)$" experiments into the linear regression. The conditions of these experiments were identical to the dark experiments except for the fact that we injected enough O_3 to convert 100% of NO into NO_2. Thus, they can be considered as three extra dark experiments. These three experiments presented three data points at $f(NO_2)=1$ ($1-f(NO_2)=0$) and $\delta(NO_2)-\delta(NO_x)=0\pm0.8$‰. **If we add these 3 points ((0, 0.8‰), (0, -0.1‰), (0, -0.7‰)) into Figure 2B, the unforced regression of the 8 points shows a slope of 28.5‰ with an intercept of -0.16‰. This slope is within the uncertainty of our forced linear regression slope.** The intercept here is much closer to 0 and should be originated from analytical uncertainties. Thus, we think the slope of the forced regression (28.1‰) should represent the true slope of this set of experiments.

We hope the above explanation clarified our reasons to calculate the slope by forcing the line through 0.

List of changes

1. in table 1, unit of NO, NO_2 and O_3 concentrations was changed from “ppb” to “nmol mol^{-1}”

Quantifying the nitrogen isotope effects during photochemical equilibrium between NO and NO_2: implications for $\delta^{15}N$ in tropospheric reactive nitrogen

Jianghanyang Li[1], Xuan Zhang[2], John Orlando[2], Geoffrey Tyndall[2] and Greg Michalski[1,3]

[1.] Department of Earth, Atmospheric and Planetary Sciences, Purdue University, West Lafayette, IN, 47907
[2.] Atmospheric Chemistry Observations and Modeling Lab, National Center for Atmospheric Research, Boulder, CO, 80301
[3.] Department of Chemistry, Purdue University, West Lafayette, IN, 47907

Correspondence to: Jianghanyang Li (li2502@purdue.edu)

Abstract. Nitrogen isotope fractionations between nitrogen oxides (NO and NO_2) play a significant role in determining the nitrogen isotopic compositions ($\delta^{15}N$) of atmospheric reactive nitrogen. Both the equilibrium isotopic exchange between NO and NO_2 molecules and the isotope effects occurring during the NO_x photochemical cycle are important, but both are not well constrained. The nighttime and daytime isotopic fractionations between NO and NO_2 in an atmospheric simulation chamber at atmospherically relevant NO_x levels were measured. Then, the impact of NO_x level and NO_2 photolysis rate to the combined isotopic fractionation (equilibrium isotopic exchange and photochemical cycle) between NO and NO_2 were calculated. It was found that the isotope effects occurring during the NO_x photochemical cycle can be described using a single fractionation factor, designated the Leighton Cycle Isotope Effect (LCIE). The results showed that at room temperature, the fractionation factor of nitrogen isotopic exchange is 1.0289±0.0019, and the fractionation factor of LCIE (when O_3 solely controls the oxidation from NO to NO_2) is 0.990±0.005. The measured LCIE factor showed good agreement with previous field measurements, suggesting that it could be applied in ambient environment, although future work is needed to assess the isotopic fractionation factors of NO + $RO_2/HO_2 \rightarrow NO_2$. The results were used to model the NO-NO_2 isotopic fractionations under several NO_x conditions. The model suggested that isotopic exchange was the dominate factor when NO_x >20 nmol mol^{-1}, while LCIE was more important at low NO_x concentrations (<1 nmol mol^{-1}) and high rates of NO_2 photolysis. These findings provided a useful tool to quantify the isotopic fractionations between tropospheric NO and NO_2, which can be applied in future field observations and atmospheric chemistry models.

1. Introduction

The nitrogen isotopic composition ($\delta^{15}N$) of reactive nitrogen compounds in the atmosphere is an important tool in understanding the sources and chemistry of atmospheric NO_x ($NO+NO_2$). It has been suggested that the $\delta^{15}N$ value of atmospheric nitrate (HNO_3, nitrate aerosols and nitrate ions in the precipitation and snow) imprints the $\delta^{15}N$ value of NO_x sources (Elliott et al., 2009; Kendall et al., 2007) thus many studies have used the $\delta^{15}N$ values of atmospheric nitrate to investigate NO_x sources (Chang et al., 2018; Felix et al., 2012; Felix & Elliott, 2014; Gobel et al., 2013; Hastings et al., 2004, 2009; Morin et al., 2009; Park et al., 2018; Walters et al., 2015, 2018). However, there remain questions about how isotopic fractionations that may occur during photochemical cycling of NO_x could alter the $\delta^{15}N$ values as it partitions into NO_y (NO_y = atmospheric nitrate, NO_3, N_2O_5, HONO, etc., Chang et al., 2018; Freyer, 1991; Hastings et al., 2004; Jarvis et al., 2008; Michalski et al., 2005; Morin et al., 2009; Zong et al., 2017). Similarily, other complex reactive nitrogen chemistry, such as nitrate photolysis and re-deposition in ice and snow (Frey et al., 2009), may impact the $\delta^{15}N$ of NO_y and atmospheric nitrate. The fractionation between NO and NO_2 via isotope exchange has been suggested to be the dominant factor in determining the $\delta^{15}N$ of NO_2 and ultimately atmospheric nitrate (Freyer, 1991; Freyer et al., 1993; Savarino et al., 2013; Walters et al., 2016). However, isotopic fractionations occur in most, if not all, NO_x and NO_y reactions, while most of these are still unknown or, if calculated (Walters and Michalski, 2015), unverified by experiments. Since the atmospheric chemistry of NO_y varies significantly in different environments (e.g., polluted vs. pristine, night vs. day), the isotopic fractionations associated with NO_y chemistry are also likely to vary in different environments. These unknowns could potentially bias conclusions about NO_x source apportionment reached when using nitrogen isotopes. Therefore, understanding the isotopic

fractionations between NO and NO_2 during photochemical cycling could improve our understanding of the relative role of sources versus chemistry for controlling the $\delta^{15}N$ variations of atmospheric NO_2 and nitrate.

In general, there are three types of isotopic fractionation effects associated with NO_x chemistry (Fig. 1A). The first type is the equilibrium isotopic effect (EIE), i.e., isotope exchange between two compounds without forming new molecules (Urey, 1947, Bigeleisen and Mayer, 1947), which for nitrogen isotopes in the NO_x system is the $^{15}NO + {}^{14}NO_2 \leftrightarrow {}^{14}NO + {}^{15}NO_2$ exchange reaction (Begun and Melton, 1956, Walters et al., 2016). The second type is the kinetic isotopic effect (KIE) associated with difference in isotopologue rate coefficients during unidirectional reactions (Bigeleisen & Wolfsberg, 1957). In the NO_x system this KIE would manifest in the oxidation of NO into NO_2 by $O_3/HO_2/RO_2$. The third type is the photochemical isotope fractionation effect (PHIFE, Miller & Yung, 2000), which for NO_x is the isotopic fractionation associated with NO_2 photolysis. All three fractionations could impact the $\delta^{15}N$ value of NO_2, and consequently atmospheric nitrate, but the relative importance of each may vary.

The limited number of studies on the EIE in the NO_x cycle have significant uncertainties. Discrepancies in the EIE for $^{15}NO + {}^{14}NO_2 \leftrightarrow {}^{14}NO + {}^{15}NO_2$ have been noted in several studies. Theoretical calculations predicted isotope fractionation factors (α) ranging from 1.035 to 1.042 at room temperature (Begun & Fletcher, 1960; Monse et al., 1969; Walters & Michalski, 2015) due to the different approximations used to calculate harmonic frequencies in each study. Likewise, two separate experiments measured different room temperature fractionation factors of 1.028±0.002 (Begun & Melton, 1956) and 1.0356±0.0015 (Walters et al., 2016). A concern in both experiments is that they were conducted in small chambers with high NO_x concentrations (hundreds of μmol mol^{-1}), significantly higher than typical ambient atmospheric NO_x levels

(usually less than 0.1 μmol mol^{-1}). Whether the isotopic fractionation factors determined by these experiments are applicable in the ambient environment is uncertain because of possible wall effects and formation of higher oxides, notably N_2O_4 and N_2O_3 at these high NO_x concentrations.

Even less research has examined the KIE and PHIFE occurring during NO_x cycling. The KIE of NO + O_3 has been theoretically calculated (Walters and Michalski, 2016) but has not been experimentally verified. The NO_2 PHIFE has not been experimentally determined or theoretically calculated. As a result, field observation studies often overlook the effects of PHIFE and KIE. Freyer et al. (1993) measured NO_x concentrations and the $\delta^{15}N$ values of NO_2 over a 1-year period at Julich, Germany and inferred a combined NO_x isotope fractionation factor (EIE+KIE+PHIFE) of 1.018±0.001. Freyer et al. (1993) suggested that the NO_x photochemical cycle (KIE and PHIFE) tends to diminish the equilibrium isotopic fractionation (EIE) between NO and NO_2. Even if this approach were valid, applying this single fractionation factor elsewhere, where NO_x, O_3 concentrations and actinic fluxes are different, would be tenuous given that these factors may influence the relative importance of EIE, KIE and PHIFE (Hastings et al., 2004; Walters et al., 2016). Therefore, to quantify the overall isotopic fractionations between NO and NO_2 at various tropospheric conditions, it is crucial to know 1) isotopic fractionation factors of EIE, KIE and PHIFE individually and 2) the relative importance of each factor under various conditions.

In this work, we aim to quantify the nitrogen isotope fractionation factors between NO and NO_2 at photochemical equilibrium. First, we measure the N isotope fractionations between NO and NO_2 in an atmospheric simulation chamber at atmospherically relevant NO_x levels. Then, we provide mathematical solutions to assess the impact of NO_x level and NO_2 photolysis rate ($j(NO_2)$) to the relative importance of EIE, KIE and PHIFE. Subsequently we use the solutions and chamber measurements to calculate the isotopic fractionation factors of EIE, KIE and PHIFE. Lastly, using

the calculated fractionation factors and the equations, we model the NO-NO_2 isotopic fractionations at several sites to illustrate the behavior of $\delta^{15}N$ values of NO_x in the ambient environment.

2. Methods

The experiments were conducted using a 10 m^3 Atmospheric Simulation Chamber at the National Center for Atmospheric Research (see descriptions in Appendix A and Zhang et al. (2018)). A set of mass flow controllers was used to inject NO and O_3 into the chamber. NO was injected at 1 L min^{-1} from an in-house NO/N_2 cylinder (133.16 μmol mol^{-1} NO in ultra-pure N_2), and O_3 was generated by flowing 5 L min^{-1} zero-air through a flow tube equipped with a UV Pen-Ray lamp (UVP LLC., CA) into the chamber. NO and NO_2 concentrations were monitored in real time by chemiluminescence with a detection limit of 0.5 nmol mol^{-1} (model CLD 88Y, Eco Physics, MI) as were O_3 concentrations using an UV absorption spectroscopy with a detection limit of 0.5 nmol mol^{-1} (model 49, Thermo Scientific, CO). In each experiment, the actual amounts of NO and O_3 injected were calculated using measured NO_x and O_3 concentrations after steady state was reached (usually within 1 h). The wall loss rate of NO_2 was tested by monitoring O_3 (29 nmol mol^{-1}) and NO_x (62 nmol mol^{-1}) over a 4-hour period. After the NO and NO_2 concentrations reached steady state, no decrease in NO_2 concentrations was observed showing that chamber wall loss was negligible.

Three experiments were conducted to measure the $\delta^{15}N$ value of the tank NO (i.e., the $\delta^{15}N$ value of total NO_x). In each of these experiments, a certain amount of O_3 was first injected into the chamber, then approximately the same amount of NO was injected into the chamber to ensure 100% of the NO_x was in the form of NO_2 with little O_3 (<15 nmol mol^{-1}) remaining in the chamber, such

that the O_3+NO_2 reaction was negligible. The NO_2 in the chamber was then collected and its $\delta^{15}N$ value measured, which equates to the $\delta^{15}N$ value of the tank NO.

Two sets of experiments were conducted to separately investigate the EIE, KIE and PHIFE. The first set of experiments was conducted in the dark. In each of these dark experiments, a range of NO and O_3 ([O_3]<[NO]) was injected into the chamber to produce NO-NO_2 mixtures with [NO]/[NO_2] ratios ranging from 0.43 to 1.17. The N isotopes of these mixtures were used to investigate the EIE between NO and NO_2. The second set of experiments was conducted under irradiation of UV lights (300-500 nm, see Appendix A for irradiation spectrum). Under such conditions, NO, NO_2 and O_3 reached photochemical steady state, which combined the isotopic effects of EIE, KIE and PHIFE.

In all experiments, the concentrations of NO, NO_2 and O_3 were allowed to reach steady state, and the product NO_2 was collected from the chamber using a honeycomb denuder tube. After the NO, NO_2 and O_3 concentrations reached steady-state, well-mixed chamber air was drawn out through a 40 cm long Norprene Thermoplastic tubing at 10 L min^{-1} and passed through a honeycomb denuder system (Chemcomb 3500, Thermo Scientific). Based on flow rate, the NO_2 residence time in the was less than 0.5 second, thus in the light-on experiments where NO and O_3 coexisted, the NO_2 produced inside the transfer tube through NO+O_3 reactions should be <0.03 nmol mol^{-1} (using the upper limit of NO and O_3 concentrations in our experiments). The honeycomb denuder system consisted of two honeycomb denuder tubes connected in series. Each honeycomb denuder tube is a glass cylinder of 38 mm long, 47 mm in diameter, and consist of 212 hexagonal tubes with inner diameters of 2 mm. Before collecting samples, each denuder tube was coated with a solution of 10% KOH and 25% guaiacol in methanol and then dried by flowing N_2 gas through the denuder tube for 15 seconds (Williams and Grosjean, 1990, Walters et al., 2016).

148 The NO_2 reacted with guaiacol coating and was converted into NO_2^- that was retained on the
149 denuder tube wall (Williams and Grosjean, 1990). NO was inert to the denuder tube coating: a
150 control experiment sampled pure NO using the denuder tubes, which did not show any measurable
151 NO_2^-. The NO_2 collection efficiency of a single honeycomb denuder tube was tested in another
152 control experiment: air containing 66 nmol mol^{-1} of NO_2 was drawn out of the chamber through a
153 denuder tube, and the NO_2 concentration at the exit of the tube holder was measured and found to
154 be below the detection limit (<1 nmol mol^{-1}), suggesting the collection efficiency was nearly 100%
155 when [NO_2] <66 nmol mol^{-1}. Furthermore, when the denuder system consisted of two denuder
156 tubes in series and NO_2^- in the second denuder was below the detection limit indicating trivial NO_2
157 breakthrough. Each NO_2 collection lasted for 0.5-3 hours in order to collect enough NO_2^- for
158 isotopic analysis (at least 300 nmol). After collection, the NO_2^- was leached from each denuder
159 tube by rinsing thoroughly with 10 ml deionized water into a clean polypropylene container and
160 stored frozen until isotopic analysis. Isotopic analysis was conducted at Purdue Stable Isotope
161 Laboratory. For each sample, approximately 50 nmol of the NO_2^- extract was mixed with 2 M
162 sodium azide solution in acetic acid buffer in an air-tight glass vial, then shaken overnight to
163 completely reduce all the NO_2^- to $N_2O_{(g)}$ (Casciotti & McIlvin, 2007; McIlvin & Altabet, 2005).
164 The product N_2O was directed into a Thermo GasBench equipped with cryo-trap, then the $\delta^{15}N$ of
165 the N_2O was measured using a Delta-V Isotope Ratios Mass Spectrometer. Six coated denuders
166 tubes that did not get exposed to NO_2 were also analyzed using the same chemical procedure,
167 which did not show any measurable signal on the IRMS, suggesting the blank from both sampling
168 process and the chemical conversion process was negligible. The overall analytical uncertainty for
169 $\delta^{15}N$ analysis was 0.5 ‰ (1σ) based on replicate analysis of in house NO_2^- standards.
170

3. Results and Discussions

3.1. Equilibrium Isotopic Fractionation between NO and NO_2

The equilibrium isotope fractionation factor, $\alpha(NO_2\text{-}NO)$, is the ^{15}N enrichment in NO_2 relative to NO, and is expressed as the ratio of rate constants k_2 / k_1 of two reactions:

$^{15}NO_2 + {}^{14}NO \rightarrow {}^{15}NO + {}^{14}NO_2$ R1, rate constant = k_1

$^{15}NO + {}^{14}NO_2 \rightarrow {}^{15}NO_2 + {}^{14}NO$ R2, rate constant = $k_2 = k_1\ \alpha(NO_2\text{-}NO)$

where k_1 is the rate constant of the isotopic exchange, which was previously determined to be 8.14×10^{-14} $cm^3\ s^{-1}$ (Sharma et al., 1970). The reaction time required for NO-NO_2 to reach isotopic equilibrium was estimated using the exchange rate constants in a simple kinetics box model (BOXMOX, Knote et al., 2015). The model predicts that at typical NO_x concentrations used during the chamber experiments (7.7-62.4 nmol mol^{-1}), isotopic equilibrium would be reached within 15 minutes (see Appendix B). Since the sample collection usually started 1 hour after NO_x was well mixed in the chamber, there was sufficient time to reach full isotope equilibrium. The isotope equilibrium fractionation factor ($\alpha(NO_2\text{-}NO)$) is then calculated to be:

$$\alpha(NO_2 - NO) = \frac{[^{15}NO_2][^{14}NO]}{[^{14}NO_2][^{15}NO]} = \frac{R(NO_2)}{R(NO)} \quad \text{Eq. (1)}$$

where R(NO, NO_2) are the $^{15}N/^{14}N$ ratios of NO and NO_2. By definition, the $\delta^{15}N(NO)=(R(NO)/R(reference)-1)\times1000$ ‰ and $\delta^{15}N(NO_2)=(R(NO_2)/R(reference)-1)\times1000$ ‰, but hereafter, the $\delta^{15}N$ values of NO, NO_2 and NO_x will be referred as $\delta(NO)$, $\delta(NO_2)$ and $\delta(NO_x)$, respectively. Eq. (1) leads to:

$$\delta(NO_2) - \delta(NO) = (\alpha(NO_2 - NO) - 1)\ (1 + \delta(NO)) \quad \text{Eq. (2)}$$

Using Eq. (2) and applying NO_x isotopic mass balance ($\delta(NO_x)=f(NO_2)\delta(NO_2)+(1-f(NO_2))\delta(NO)$, $f(NO_2)=[NO_2]/([NO]+[NO_2])$) yields:

$$\frac{\delta(NO_2)-\delta(NO_x)}{1+\delta(NO_2)} = \frac{\alpha(NO_2-NO)-1}{\alpha(NO_2-NO)}\left(1 - f(NO_2)\right) \quad \text{Eq. (3)}$$

Here, $\delta(NO_x)$ equals to the $\delta^{15}N$ value of the cylinder NO and $f(NO_2)$ is the molar fraction of NO_2 with respect to total NO_x. Three experiments (Table 1) that measured $\delta(NO_x)$ showed consistent $\delta(NO_x)$ values of (-58.7±0.8) ‰ (n = 3), indicating $\delta(NO_x)$ remained unchanged throughout the experiments (as expected for isotope mass balance). Thus, the $\delta(NO_x)$ can be treated as a constant in Eq. (3), and the linear regression of $(\delta(NO_2)-\delta(NO_x))/(1+\delta(NO_2))$ versus $1-f(NO_2)$ should have an intercept of 0 and a slope of $(\alpha(NO_2\text{-}NO)-1)/\alpha(NO_2\text{-}NO)$.

The plot of $(\delta(NO_2)-\delta(NO_x))/(1+\delta(NO_2))$ as a function of $1-f(NO_2)$ values from five experiments yields an $\alpha(NO_2\text{-}NO)$ value of 1.0289±0.0019 at room temperature (Fig. 1B and Table 1). This fractionation factor is comparable to previously measured values but with some differences. Our result agrees well with the $\alpha(NO_2\text{-}NO)$ value of 1.028±0.002 obtained by Begun and Melton (1956) at room temperature. However, Walters et al., (2016) determined the $\alpha(NO_2\text{-}NO)$ values of $NO\text{-}NO_2$ exchange in a 1-liter reaction vessel, which showed a slightly higher $\alpha(NO_2\text{-}NO)$ value of 1.035. This discrepancy might originate from rapid heterogeneous reactions on the wall of the reaction vessel at high NO_x concentrations and the small chamber size used by Walters et al. (2016). They used a reaction vessel made of Pyrex, which is known to absorb water (Do Remus et al., 1983; Takei et al., 1997) that can react with NO_2 forming HONO, HNO_3 and other N compounds. Additionally, previous studies have suggested that Pyrex walls enhance the formation rate of N_2O_4 by over an order of magnitude (Barney & Finlayson-Pitts, 2000; Saliba et al., 2001), which at isotopic equilibrium is enriched in ^{15}N compared to NO and NO_2 (Walters & Michalski, 2015). Therefore, their measured $\alpha(NO_2\text{-}NO)$ might be slightly higher than the actual $\alpha(NO_2\text{-}NO)$ value. In this work, the 10 m^3 chamber has a much smaller surface to volume ratio relative to Walters et al. (2016) which minimizes wall effects, and the walls were made of Teflon that minimize NO_2 surface reactivity, which was evidenced by the NO_2 wall loss control

217 experiment. Furthermore, the low NO_x mixing ratios in our experiments minimized N_2O_4 and N_2O_3
218 formation. At NO and NO_2 concentrations of 50 nmol mol^{-1} the steady state concentrations of N_2O_4
219 and N_2O_3 were calculated to be 0.014 and 0.001 pmol mol^{-1}, respectively (Atkinson et al., 2004).
220 Therefore, we suggest our measured $\alpha(NO_2\text{-}NO)$ value (1.0289±0.0019) may better reflect the
221 room temperature (298 K) NO-NO_2 EIE in the ambient environment.
222 Unfortunately, the chamber temperature could not be controlled so we were not able to
223 investigate the temperature dependence of the EIE. Hence, we speculate that the $\alpha(NO_2\text{-}NO)$
224 follows a similar temperature dependence pattern calculated in Walters et al. (2016). Walters et al.
225 (2016) suggested that, the $\alpha(NO_2\text{-}NO)$ value would be 0.0047 higher at 273 K and 0.002 lower at
226 310 K, relative to room temperature (298 K). Using this pattern and our experimentally determined
227 data, we suggest the $\alpha(NO_2\text{-}NO)$ values at 273 K, 298 K and 310 K are 1.0336±0.0019,
228 1.0289±0.0019 and 1.0269±0.0019, respectively. This 0.0067 variation at least partially contribute
229 to the daily and seasonal variations of $\delta^{15}N$ values of NO_2 and nitrate in some areas (e.g., polar
230 regions with strong seasonal temperature variation). Thus, future investigations should be
231 conducted to verify the EIE temperature dependence.
232
233 **3.2. Kinetic isotopic fractionation of Leighton Cycle**
234 The photochemical reactions of NO_x will compete with the isotope exchange fractionations
235 between NO and NO_2. The NO-NO_2 photochemical cycle in the chamber was controlled by the
236 Leighton cycle: NO_2 photolysis and the NO + O_3 reaction. This is because there were no VOCs in
237 the chamber so no RO_2 was produced, which excludes the NO + RO_2 reaction. Likewise, the low
238 water vapor content (RH<10%) and the minor flux of photons < 310 nm results in minimal OH
239 production and hence little HO_2 formation and subsequently trivial amount of NO_2 would be

formed by NO + HO_2. Applying these limiting assumptions, the EIE between NO and NO_2 (R1-R2) were only competing with the KIE (R3-R4) and the PHIFE in R5-R6:

$^{14}NO_2 \rightarrow {}^{14}NO + O$ R3, rate constant=$j(NO_2)$

$^{15}NO_2 \rightarrow {}^{15}NO + O$ R4, rate constant=$j(NO_2)\ \alpha_1$

$^{14}NO + O_3 \rightarrow {}^{14}NO_2 + O_2$ R5, rate constant=k_5

$^{15}NO + O_3 \rightarrow {}^{15}NO_2 + O_2$ R6, rate constant=$k_5\ \alpha_2$

In which $j(NO_2)$ is the NO_2 photolysis rate (1.4×10^{-3} s^{-1} in these experiments), k_5 is the rate constant for the $NO+O_3$ reaction (1.73×10^{-14} cm^3 s^{-1}, Atkinson et al., 2004), and $\alpha_{1,2}$ are isotopic fractionation factors for the two reactions. Previous studies (Freyer et al., 1993; Walters et al., 2016) have attempted to assess the competition between EIE (R1-R2), KIE and PHIFE (R3-R6), but none of them quantified the relative importance of the two processes, nor were α_1 or α_2 values experimentally determined. Here we provide the mathematical solution of EIE, KIE and PHIFE to illustrate how R1-R6 affect the isotopic fractionations between NO and NO_2.

First, the NO_2 lifetime with respect to isotopic exchange with NO ($\tau_{exchange}$) and photolysis (τ_{photo}) was determined:

$$\tau_{exchange} = \frac{1}{k_1\,[NO]} \quad \text{Eq. (4)}$$

$$\tau_{photo} = \frac{1}{j(NO_2)} \quad \text{Eq. (5)}$$

We then define an A factor:

$$A = \begin{cases} \frac{\tau_{exchange}}{\tau_{photo}} & \text{when } j(NO_2) \neq 0 \\ 0 & \text{when } j(NO_2) = 0 \end{cases} \quad \text{Eq. (6)}$$

Using R1-R6 and Eq. (1)-(6), we solved steady-state $\delta(NO_2)$ and $\delta(NO)$ values (see calculations in Appendix C). Our calculations show that the $\delta(NO_2)$-$\delta(NO)$ and $\delta(NO_2)$-$\delta(NO_x)$ values at steady state can be expressed as functions of α_1, α_2, $\alpha(NO_2\text{-}NO)$ and A:

$$\delta(NO_2) - \delta(NO) = \frac{(\alpha_2-\alpha_1)\,A+(\alpha(NO_2-NO)-1)}{\alpha_2 A+\alpha(NO_2-NO)}\left(1+\delta(NO_2)\right)$$

$$\approx \frac{(\alpha_2-\alpha_1)\,A+(\alpha(NO_2-NO)-1)}{A+1}\left(1+\delta(NO_2)\right) \quad \text{Eq. (7)}$$

$$\delta(NO_2) - \delta(NO_x) = \frac{(\alpha_2-\alpha_1)\,A+(\alpha(NO_2-NO)-1)}{\alpha_2 A+\alpha(NO_2-NO)}\,(1+\delta(NO_2))(1-f(NO_2))$$

$$\approx \frac{(\alpha_2-\alpha_1)\,A+(\alpha(NO_2-NO)-1)}{A+1}\left(1+\delta(NO_2)\right)(1-f(NO_2)) \quad \text{Eq. (8)}$$

Equation (7) shows the isotopic fractionation between NO and NO_2 ($\delta(NO_2)$-$\delta(NO)$) is mainly determined by A, the EIE factor ($\alpha(NO_2\text{-}NO)$-1) and the (α_2-α_1) factor assuming (1+$\delta(NO_2)$) is close to 1. This (α_2-α_1) represents a combination of KIE and PHIFE, suggesting they act together as one factor; therefore, we name the (α_2-α_1) factor Leighton Cycle Isotopic Effect, i.e., LCIE. Using measured $\delta(NO_2)$, $\delta(NO_x)$ values, A values (Table 1), and the previously determined $\alpha(NO_2\text{-}NO)$ value, We plot $\frac{\delta(NO_2)-\delta(NO_x)}{(1+\delta(NO_2))(1-f(NO_2))}$ (equals to $\frac{\delta(NO_2)-\delta(NO)}{(1+\delta(NO_2))}$) against A value and use Equations (7) and (8) to estimate the (α_2-α_1) value (Fig. 1C). The plot shows that the best fit for the LCIE factor is (-10±5) ‰ (Rooted Mean Square Error, RMSE, was lowest when α_2-α_1 =-10‰). The uncertainties in the LCIE factor are relatively higher than that of the EIE factor, mainly because of the accumulated analytical uncertainties at low NO_x and O_3 concentrations, and low A values (0.10-0.28) due to the relatively low $j(NO_2)$ value (1.4×10^{-3} s^{-1}) under the chamber irradiation conditions.

This LCIE factor determined in our experiments is in good agreement with theoretical calculations. Walters and Michalski (2016) previously used an *ab initio* approach to determine an

α_2 value of 0.9933 at room temperature, 0.9943 at 237 K and 0.9929 at 310 K. The total variation of α_2 values from 273 K to 310 K is only 1.4 ‰, significantly smaller than our experimental uncertainty (±5 ‰). The α_1 value was calculated using a ZPE shift model (Miller & Yung, 2000) to calculate the isotopic fractionation of NO_2 by photolysis. Briefly, this model assumes both isotopologues have the same quantum yield function and the PHIFE was only caused by the differences in the $^{15}NO_2$ and $^{14}NO_2$ absorption cross-section as a function of wavelength, thus α_1 values do not vary by temperature. The $^{15}NO_2$ absorption cross-section was calculated by shifting the $^{14}NO_2$ absorption cross-section by the $^{15}NO_2$ zero-point energy (Michalski et al., 2004). When the ZPE shift model was used with the irradiation spectrum of the chamber lights, the resulting α_1 value was 1.0023. Therefore, the theoretically predicted α_2-α_1 value should be -0.0090, i.e., (-9.0±0.7) ‰ when temperature ranges from 273 K to 310 K. This result shows excellent agreement with our experimentally determined room temperature α_2-α_1 value of (-10±5) ‰.

This model was then used to evaluate the variations of α_1 value to different lighting conditions. The TUV model (TUV5.3.2, Madronich & Flocke, 1999) was used to calculate the solar wavelength spectrum at three different conditions: early morning/late afternoon (solar zenith angle=85 degree), mid-morning/afternoon (solar zenith angle=45 degree), noon (solar zenith angle=0 degree). These spectrums were used in the ZPE shift model to calculate the α_1 values, which are 1.0025, 1.0028, and 1.0029 at solar zenith angles of 85, 45 and 0 degree, respectively. These values, along with the predicted α_1 value in the chamber, showed a total span of 0.6‰ (1.0026±0.0003), which is again significantly smaller than our measured uncertainty. Therefore, we suggest that our experimentally determined LCIE factor ((-10±5) ‰) can be used in most tropospheric solar irradiation spectrums.

The equations can also be applied in tropospheric environments to calculate the combined isotopic fractionations of EIE and LCIE for NO and NO_2. First, the NO_2 sink reactions (mainly NO_2+OH in the daytime) are at least 2-3 orders of magnitude slower than the Leighton cycle and the NO-NO_2 isotope exchange reactions (Walters et al., 2016), therefore their effects on the $\delta(NO_2)$ should be minor. Second, although the conversion of NO into NO_2 in the ambient environment is also controlled by NO + RO_2 and HO_2 in addition to NO+O_3 (e.g., King et al., 2001), Eq. (7) still showed good agreement with field observations in previous studies. Freyer et al. (1993) determined the annual average daytime $\delta(NO_2)$-$\delta(NO)$ at Julich, Germany along with average daytime NO concentration (9 nmol mol^{-1}, similar to our experimental conditions) to be (+18.03±0.98) ‰. Using Eq. (7), assuming the daytime average $j(NO_2)$ value throughout the year was $(5.0\pm1.0)\times10^{-3}$, and a calculated A value from measured NO_x concentration ranged from 0.22-0.33, the average NO-NO_2 fractionation factor was calculated to be (+19.8±1.4) ‰ (Fig. 1C), in excellent agreement with the measurements in the present study. This agreement suggests the NO+RO_2/HO_2 reactions might have similar fractionation factors as NO+O_3. Therefore, we suggest Eq. (7) and (8) can be used to estimate the isotopic fractionations between NO and NO_2 in the troposphere.

3.3 Calculating nitrogen isotopic fractionations of NO-NO_2

First, Eq. (7) was used to calculate the $\Delta(NO_2\text{-}NO) = \delta(NO_2)\text{-}\delta(NO)$ at a wide range of NO_x concentrations, $f(NO_2)$ and $j(NO_2)$ values (Fig. 2A-D), assuming $(1+\delta(NO_2)) \approx 1$. $j(NO_2)$ values of 0 s^{-1} (Fig. 2A), 1.4×10^{-3} s^{-1} (Fig. 2B), 5×10^{-3} s^{-1} (Fig. 2C) and 1×10^{-2} s^{-1} (Fig. 2D) were selected to represent nighttime, dawn (as well as the laboratory conditions of our experiments), daytime average and noon, respectively. Each panel represented a fixed $j(NO_2)$ value, and the

$\Delta(NO_2\text{-}NO)$ values were calculated as a function of the A value, which was derived from NO_x concentration and $f(NO_2)$. The A values have a large span, from 0 to 500, depending on the $j(NO_2)$ value and the NO concentration. When A=0 ($j(NO_2)$=0) and $f(NO_2)$<1 (meaning NO-NO_2 coexist and $[O_3]$=0), Eq. (7) and (8) become Eq. (2) and (3), showing the EIE was the sole factor, the $\Delta(NO_2\text{-}NO)$ values were solely controlled by EIE which has a constant value of +28.9 ‰ at 298K (Fig. 2A). When $j(NO_2)$ >0, the calculated $\Delta(NO_2\text{-}NO)$ values showed a wide range from -10.0 ‰ (controlled by LCIE factor: $\alpha_2\text{-}\alpha_1$=-10 ‰) to +28.9 ‰ (controlled by EIE factor: $\alpha(NO_2\text{-}NO)\text{-}1$ = +28.9 ‰). Fig. 2B-D display the transition from a LCIE-dominated regime to an EIE-dominated regime. The LCIE-dominated regime is characterized by low $[NO_x]$ (<50 pmol mol^{-1}), representing remote ocean areas and polar regions (Beine et al., 2002; Custard et al., 2015). At this range the A value can be greater than 200, thus Eq. (7) can be simplified as: $\Delta(NO_2\text{-}NO) = \alpha_2\text{-}\alpha_1$, suggesting the LCIE almost exclusively controls the NO-NO_2 isotopic fractionation. The $\Delta(NO_2\text{-}NO)$ values of these regions are predicted to be <0 ‰ during most time of the day and < -5 ‰ at noon. On the other hand, the EIE-dominated regime was characterized by high $[NO_x]$ (>20 nmol mol^{-1}) and low $f(NO_2)$ (< 0.6), representative of regions with intensive NO emissions, e.g., near roadside or stack plumes (Clapp & Jenkin, 2001; Kimbrough et al., 2017). In this case, the $\tau_{exchange}$ are relatively short (10-50 s) compared to the τ_{photo} (approximately 100 s at noon and 1000 s at dawn), therefore the A values are small (0.01-0.5). The EIE factor in this regime thus is much more important than the LCIE factor, resulting in high $\Delta(NO_2\text{-}NO)$ values (>20 ‰). Between the two regimes, both EIE and LCIE are competitive and therefore it is necessary to use Eq. (7) to quantify the $\Delta(NO_2\text{-}NO)$ values.

Fig. 2 also implies that changes in the $j(NO_2)$ value can cause the diurnal variations in $\Delta(NO_2\text{-}NO)$ values. Changing $j(NO_2)$ would affect the value of A and consequently the NO-NO_2

isotopic fractionations in two ways: 1) changes in $j(NO_2)$ value would change the photolysis intensity, therefore the τ_{photo} value; 2) in addition, changes in $j(NO_2)$ value would also alter the steady state NO concentration, therefore changing the $\tau_{exchange}$ (Fig. 2C). The combined effect of these two factors on the A value varies along with the atmospheric conditions, and thus needs to be carefully calculated using NO_x concentration data and atmospheric chemistry models.

We then calculated the differences of $\delta^{15}N$ values between NO_2 and total NO_x, e.g. $\Delta(NO_2\text{-}NO_x) = \delta(NO_2)\text{-}\delta(NO_x)$ in Fig. 2E-H. Since $\Delta(NO_2\text{-}NO_x)$ are connected through the observed $\delta^{15}N$ of NO_2 (or nitrate) to the $\delta^{15}N$ of NO_x sources, this term might be useful in field studies (e.g., Chang et al., 2018; Zong et al., 2017). The calculated $\Delta(NO_2\text{-}NO_x)$ values (Fig. 2E-H) also showed a LCIE-dominated regime at low $[NO_x]$ and an EIE-dominated regime at high $[NO_x]$. The $\Delta(NO_2\text{-}NO_x)$ values were dampened by the $1\text{-}f(NO_2)$ factor comparing to $\Delta(NO_2\text{-NO})$, as shown in Eq. (3) and (8): $\Delta(NO_2\text{-}NO_x) = \Delta(NO_2\text{-NO})\,(1\text{-}f(NO_2))$. At high $f(NO_2)$ values (>0.8), the differences between $\delta(NO_2)$ and $\delta(NO_x)$ were less than 5 ‰, thus the measured $\delta(NO_2)$ values were similar to $\delta(NO_x)$, although the isotopic fractionation between NO and NO_2 could be noteworthy. Some ambient environments with significant NO emissions or high NO_2 photolysis rates usually have $f(NO_2)$ values between 0.4-0.8 (Mazzeo et al., 2005; Vicars et al., 2013). In this scenario, the $\Delta(NO_2\text{-}NO_x)$ values in Fig. 2F-H showed wide ranges of -4.8 ‰ to +15.6 ‰, -6.0 ‰ to +15.0 ‰, and -6.3 ‰ to +14.2 ‰ at $j(NO_2)=1.4\times10^{-3}$ s^{-1}, 5×10^{-3} s^{-1}, 1×10^{-2} s^{-1}, respectively. These significant differences again highlighted the importance of both LCIE and EIE (Eq. (7) and (8)) in calculating the $\Delta(NO_2\text{-}NO_x)$. In the following discussion, we assume 1) the α_1 value remain constant (see discussion above), 2) the $NO+RO_2/HO_2$ reactions have the same fractionation factors (α_2) as $NO+O_3$, and 3) both EIE and LCIE do not display significant temperature dependence, then use

370 Equations (7) and (8) and this laboratory determined LCIE factor (-10 ‰) to calculate the nitrogen
371 isotopic fractionation between NO and NO_2 at various tropospheric atmospheric conditions.
372
373 **4. Implications**
374 The daily variations of $\Delta(NO_2\text{-}NO_x)$ values at two roadside NO_x monitoring sites were
375 predicted to demonstrate the effects of NO_x concentrations to the NO-NO_2 isotopic fractionations.
376 Hourly NO and NO_2 concentrations were acquired from a roadside site at Anaheim, CA
377 (https://www.arb.ca.gov) and an urban site at Evansville, IN (http://idem.tx.sutron.com) on July
378 25, 2018. The hourly $j(NO_2)$ values output from the TUV model (Madronich & Flocke, 1999) at
379 these locations was used to calculate the daily variations of $\Delta(NO_2\text{-}NO_x)$ values (Fig. 3A, B) by
380 applying Eq. (8) and assuming $(1+\delta(NO_2)) \approx 1$. Hourly NO_x concentrations were 12-51 nmol mol^{-1}
381 at Anaheim and 9-38 nmol mol^{-1} at Evansville and the $f(NO_2)$ values at both sites did not show
382 significant daily variations (0.45±0.07 at Anaheim and 0.65±0.08 at Evansville), likely because
383 the NO_x concentrations were controlled by the high NO emissions from the road (Gao, 2007). The
384 calculated $\Delta(NO_2\text{-}NO_x)$ values using Eq. (8) showed significant diurnal variations. During the
385 nighttime, the isotopic fractionations were solely controlled by the EIE, the predicted $\Delta(NO_2\text{-}NO_x)$
386 values were (+14.5±2.0) ‰ and (+8.7±2.1) ‰ at Anaheim and Evansville, respectively. During
387 the daytime, the existence of LCIE lowered the predicted $\Delta(NO_2\text{-}NO_x)$ values to (+9.8±1.7) ‰ at
388 Anaheim and (+3.1±1.5) ‰ at Evansville while the $f(NO_2)$ values at both sites remained similar.
389 The lowest $\Delta(NO_2\text{-}NO_x)$ values for both sites (+7.0 ‰ and +1.7 ‰) occurred around noon when
390 the NO_x photolysis was the most intense. In contrast, if one neglects the LCIE factor in the daytime,
391 the $\Delta(NO_2\text{-}NO_x)$ values would be (+12.9±1.5) ‰ and (+10.0±1.6) ‰ respectively, an
392 overestimation of 3.1 ‰ and 6.9 ‰. These discrepancies suggested that the LCIE played an

393 important role in the NO-NO_2 isotopic fractionations and neglecting it could bias the NO_x source
394 apportionment using $\delta^{15}N$ of NO_2 or nitrate.

395 The role of LCIE was more important in less polluted sites. The $\Delta(NO_2\text{-}NO_x)$ values
396 calculated for a suburban site near San Diego, CA, USA, again using the hourly NO_x
397 concentrations (https://www.arb.ca.gov, Fig. 3C) and $j(NO_2)$ values calculated from the TUV
398 model. NO_x concentrations at this site varied from 1 to 9 nmol mol^{-1} and assuming $(1+\delta(NO_2)) \approx 1$.
399 During the nighttime, NO_x was in the form of NO_2 ($f(NO_2) = 1$) because O_3 concentrations were
400 higher than NO_x, thus the $\delta(NO_2)$ values should be identical to $\delta(NO_x)$ ($\Delta(NO_2\text{-}NO_x) = 0$). In the
401 daytime a certain amount of NO was produced by direct NO emission and NO_2 photolysis but the
402 $f(NO_2)$ was still high (0.73±0.08). Our calculation suggested the daytime $\Delta(NO_2\text{-}NO_x)$ values
403 should be only (+1.3±3.2) ‰ with a lowest value of -1.3 ‰. These $\Delta(NO_2\text{-}NO_x)$ values were
404 similar to the observed and modeled summer daytime $\delta(NO_2)$ values in West Lafayette, IN
405 (Walters et al., 2018), which suggest the average daytime $\Delta(NO_2\text{-}NO_x)$ values at NO_x = (3.9±1.2)
406 nmol mol^{-1} should range from +0.1 ‰ to +2.4 ‰. In this regime, we suggest the $\Delta(NO_2\text{-}NO_x)$
407 values were generally small due to the significant contribution of LCIE and high $f(NO_2)$.

408 The LCIE should be the dominant factor controlling the NO-NO_2 isotopic fractionation at
409 remote regions, resulting in a completely different diurnal pattern of $\Delta(NO_2\text{-}NO_x)$ compared with
410 the urban-suburban area. Direct hourly measurements of NO_x at remote sites are rare, thus we used
411 total NO_x concentration of 50 pmol mol^{-1}, daily O_3 concentration of 20 nmol mol^{-1} at Summit,
412 Greenland (Dibb et al., 2002; Hastings et al., 2004; Honrath et al., 1999; Yang et al., 2002), and
413 assumed $(1+\delta(NO_2)) \approx 1$ and the conversion of NO to NO_2 was completely controlled by O_3 to
414 calculate the NO/NO_2 ratios. Here the isotopes of NO_x were almost exclusively controlled by the
415 LCIE due to the high A values (>110). The $\Delta(NO_2\text{-}NO_x)$ values displayed a clear diurnal pattern

(Fig. 3D) with highest value of -0.3 ‰ in the "nighttime" (solar zenith angle >85 degree) and lowest value of -5.0 ‰ in the mid-day. This suggest that the isotopic fractionations between NO and NO_2 were almost completely controlled by LCIE at remote regions, when NO_x concentrations were <0.1 nmol mol^{-1}. However, since the isotopic fractionation factors of nitrate-formation reactions (NO_2+OH, NO_3+HC, N_2O_5+H_2O) are still unknown, more studies are needed to fully explain the daily and seasonal variations of $\delta(NO_3^-)$ at remote regions.

Nevertheless, our results have a few limitations. First, currently there are very few field observations that can be used to evaluate our model, therefore, future field observations that measure the $\delta^{15}N$ values of ambient NO and NO_2 should be carried out to test our model. Second, more work, including theoretical and experimental studies, is needed to investigate the isotope fractionation factors occurring during the conversion from NO_x to NO_y and nitrate: in the NO_y cycle, EIE (isotopic exchange between NO_2, NO_3 and N_2O_5), KIE (formation of NO_3, N_2O_5 and nitrate) and PHIFE (photolysis of NO_3, N_2O_5, HONO and sometimes nitrate) may also exist and be relevant for the $\delta^{15}N$ of HNO_3 and HONO. In particular, the N isotope fractionation occurring during the NO_2 + OH → HNO_3 reaction needs investigation. Such studies could help us modeling the isotopic fractionation between NO_x emission and nitrate, and eventually enable us to analyze the $\delta^{15}N$ value of NO_x emission by measuring the $\delta^{15}N$ values of nitrate aerosols and nitrate in wet depositions. Third, our discussion only focuses on the reactive nitrogen chemistry in the troposphere, however, the nitrogen chemistry in the stratosphere is drastically different from the tropospheric chemistry, thus future studies are also needed to investigate the isotopic fractionations in the stratospheric nitrogen chemistry. Last, the temperature dependence of both EIE and LCIE needs to be carefully investigated, because of the wide range of temperature in both troposphere and stratosphere. Changes in temperature could alter the isotopic fractionation factors of both EIE

and LCIE, as well as contribute to the seasonality of isotopic fractionations between NO_x and NO_y molecules.

5. Conclusions

The effect of NO_x photochemistry on the nitrogen isotopic fractionations between NO and NO_2 was investigated. We first measured the isotopic fractionations between NO and NO_2 and provided mathematical solutions to assess the impact of NO_x level and NO_2 photolysis rate ($j(NO_2)$) to the relative importance of EIE and LCIE. The EIE and LCIE isotope fractionation factors, at room temperature, were determined to be 1.0289±0.0019 and 0.990±0.005, respectively. These calculations and measurements can be used to determine the steady state $\Delta(NO_2\text{-}NO)$ and $\Delta(NO_2\text{-}NO_x)$ values at room temperature. Subsequently we applied our equations to polluted, clean and remote sites to model the daily variations of $\Delta(NO_2\text{-}NO_x)$ values. We found that the $\Delta(NO_2\text{-}NO_x)$ values could vary from over +20 ‰ to less than -5 ‰ depending on the environment: in general, the role of LCIE becoming more important at low NO_x concentrations, which tend to decrease the $\Delta(NO_2\text{-}NO_x)$ values. Our work provided a mathematical approach to quantify the nitrogen isotopic fractionations between NO and NO_2 that can be applied to many tropospheric environments, which could help interpret the measured $\delta^{15}N$ values of NO_2 and nitrate in field observation studies.

Acknowledgement

We thank NCAR's Advanced Study Program granted to Jianghanyang Li. The National Center for Atmospheric Research is operated by the University Corporation for Atmospheric Research, under the sponsorship of the National Science Foundation. We also thank funding

support from Purdue Climate Change Research Center and A. H. Ismail Interdisciplinary Program Doctoral Research Travel Award granted by Purdue University.

Data Availability

Data acquired from this study was deposited at Open Sciences Framework (Li, 2019, DOI 10.17605/OSF.IO/JW8HU).

Author contribution

J. Li and G. Michalski designed the experiments, X. Zhang and J. Li conducted the experiments. X. Zhang, G. Michalski, J. Orlando and G. Tyndall helped J. Li in interpreting the results. The manuscript was written by J. Li and all the authors have contributed during the revision of this manuscript.

Competing interest

The authors declare no competing interest.

References:

Atkinson, R., Baulch, D. L., Cox, R. A., Crowley, J. N., Hampson, R. F., Hynes, R. G., Jenkin, M. E., Rossi, M. J., and Troe, J. (2004). Evaluated kinetic and photochemical data for atmospheric chemistry: Volume I-gas phase reactions of O_x, HO_x, NO_x and SO_x. Atmospheric chemistry and physics, 4(6), 1461-1738. https://doi.org/10.5194/acp-4-1461-2004, 2004.

Barney, W. S., & Finlayson-Pitts, B. J. (2000). Enhancement of N_2O_4 on porous glass at room temperature: A key intermediate in the heterogeneous hydrolysis of NO_2? The Journal of Physical Chemistry A, 104(2), 171–175. https://doi.org/10.1021/jp993169b

Begun, G. M., & Fletcher, W. H. (1960). Partition function ratios for molecules containing nitrogen isotopes. The Journal of Chemical Physics, 33(4), 1083–1085. https://doi.org/10.1063/1.1731338

Begun, G. M., & Melton, C. E. (1956). Nitrogen isotopic fractionation between NO and NO_2 and mass discrimination in mass analysis of NO_2. The Journal of Chemical Physics, 25(6), 1292–1293. https://doi.org/10.1063/1.1743215

Beine, H. J., Honrath, R. E., Dominé, F., Simpson, W. R., & Fuentes, J. D. (2002). NO_x during background and ozone depletion periods at Alert: Fluxes above the snow surface. Journal of Geophysical Research: Atmospheres, 107(D21), ACH-7. https://doi.org/10.1029/2002JD002082

Bigeleisen, J., & Mayer, M. G. (1947). Calculation of equilibrium constants for isotopic exchange reactions. The Journal of Chemical Physics, 15(5), 261-267. https://doi.org/10.1063/1.1746492

Bigeleisen, J., & Wolfsberg, M. (1957). Theoretical and experimental aspects of isotope effects in chemical kinetics. Advances in Chemical Physics, 15–76. https://doi.org/10.1002/9780470143476.ch2

Casciotti, K. L., & McIlvin, M. R. (2007). Isotopic analyses of nitrate and nitrite from reference mixtures and application to Eastern Tropical North Pacific waters. Marine Chemistry, 107(2), 184–201. https://doi.org/10.1016/j.marchem.2007.06.021

Chang, Y., Zhang, Y., Tian, C., Zhang, S., Ma, X., Cao, F., et al. (2018). Nitrogen isotope fractionation during gas-to-particle conversion of NO_x to NO_3^- in the atmosphere–implications for isotope-based NO_x source apportionment. Atmospheric Chemistry and Physics, 18(16), 11647–11661. https://doi.org/10.5194/acp-18-11647-2018, 2018.

Clapp, L. J., & Jenkin, M. E. (2001). Analysis of the relationship between ambient levels of O_3, NO_2 and NO as a function of NO_x in the UK. Atmospheric Environment, 35(36), 6391–6405. https://doi.org/10.1016/S1352-2310(01)00378-8

Custard, K. D., Thompson, C. R., Pratt, K. A., Shepson, P. B., Liao, J., Huey, L. G., Orlando, J. J., Weinheimer, A. J., Apel, E., Hall, S. R., Flocke, F., Mauldin, L., Hornbrook, R. S., Pöhler, D., General, S., Zielcke, J., Simpson, W. R., Platt, U., Fried, A., Weibring, P., Sive, B. C., Ullmann, K., Cantrell, C., Knapp, D. J., and Montzka, D. D.: The NOx dependence of bromine chemistry in the Arctic atmospheric boundary layer, Atmos. Chem. Phys., 15, 10799–10809, https://doi.org/10.5194/acp-15-10799-2015, 2015.

Dibb, J. E., Arsenault, M., Peterson, M. C., & Honrath, R. E. (2002). Fast nitrogen oxide photochemistry in Summit, Greenland snow. Atmospheric Environment, 36(15–16), 2501–2511. https://doi.org/10.1016/S1352-2310(02)00130-9

Do Remus, R. H., Mehrotra, Y., Lanford, W. A., & Burman, C. (1983). Reaction of water with glass: influence of a transformed surface layer. Journal of Materials Science, 18(2), 612–622. https://doi.org/10.1007/BF00560651

Elliott, E. M., Kendall, C., Boyer, E. W., Burns, D. A., Lear, G. G., Golden, H. E., Harlin, K., Bytnerowicz, A., Butler, T. J., and Glatz, R. (2009). Dual nitrate isotopes in dry deposition: Utility for partitioning NO_x source contributions to landscape nitrogen deposition. Journal of Geophysical Research: Biogeosciences, 114(G4), G04020. https://doi.org/10.1029/2008JG000889

Felix, J. D., & Elliott, E. M. (2014). Isotopic composition of passively collected nitrogen dioxide emissions: Vehicle, soil and livestock source signatures. Atmospheric Environment, 92, 359–366. https://doi.org/10.1016/j.atmosenv.2014.04.005

Felix, J. D., Elliott, E. M., & Shaw, S. L. (2012). Nitrogen isotopic composition of coal-fired power plant NO_x: influence of emission controls and implications for global emission inventories. Environmental Science & Technology, 46(6), 3528–3535. https://doi.org/10.1021/es203355v

Frey, M. M., Savarino, J., Morin, S., Erbland, J., & Martins, J. M. F. (2009). Photolysis imprint in the nitrate stable isotope signal in snow and atmosphere of East Antarctica and implications for reactive nitrogen cycling. Atmos. Chem. Phys, 9, 8681-8696. https://doi.org/10.5194/acp-9-8681-2009, 2009.

Freyer, H. D. (1991). Seasonal variation of $^{15}N/^{14}N$ ratios in atmospheric nitrate species. Tellus B, 43(1), 30–44. https://doi.org/10.1034/j.1600-0889.1991.00003.x

Freyer, H. D., Kley, D., Volz-Thomas, A., & Kobel, K. (1993). On the interaction of isotopic exchange processes with photochemical reactions in atmospheric oxides of nitrogen. Journal of Geophysical Research: Atmospheres, 98(D8), 14791–14796. https://doi.org/10.1029/93JD00874

Gao, H. O. (2007). Day of week effects on diurnal ozone/NO_x cycles and transportation emissions in Southern California. Transportation Research Part D: Transport and Environment, 12(4), 292–305. https://doi.org/10.1016/j.trd.2007.03.004

Gobel, A. R., Altieri, K. E., Peters, A. J., Hastings, M. G., & Sigman, D. M. (2013). Insights into anthropogenic nitrogen deposition to the North Atlantic investigated using the isotopic composition of aerosol and rainwater nitrate. Geophysical Research Letters, 40(22), 5977–5982. https://doi.org/10.1002/2013GL058167

Hastings, M G, Jarvis, J. C., & Steig, E. J. (2009). Anthropogenic impacts on nitrogen isotopes of ice-core nitrate. Science, 324(5932), 1288. DOI: 10.1126/science.1170510

Hastings, M G, Steig, E. J., & Sigman, D. M. (2004). Seasonal variations in N and O isotopes of nitrate in snow at Summit, Greenland: Implications for the study of nitrate in snow and ice cores. Journal of Geophysical Research: Atmospheres, 109(D20). https://doi.org/10.1029/2004JD004991

Honrath, R. E., Peterson, M. C., Guo, S., Dibb, J. E., Shepson, P. B., & Campbell, B. (1999). Evidence of NO_x production within or upon ice particles in the Greenland snowpack. Geophysical Research Letters, 26(6), 695–698. https://doi.org/10.1029/1999GL900077

Jarvis, J. C., Steig, E. J., Hastings, M. G., & Kunasek, S. A. (2008). Influence of local photochemistry on isotopes of nitrate in Greenland snow. Geophysical Research Letters, 35(21). https://doi.org/10.1029/2008GL035551

582 Kendall, C., Elliott, E. M., & Wankel, S. D. (2007). Tracing anthropogenic inputs of nitrogen to
583 ecosystems. Stable Isotopes in Ecology and Environmental Science, 2, 375–449.
584 https://doi.org/10.1002/9780470691854.ch12
585
586 Kimbrough, S., Owen, R. C., Snyder, M., & Richmond-Bryant, J. (2017). NO to NO_2 conversion
587 rate analysis and implications for dispersion model chemistry methods using Las Vegas, Nevada
588 near-road field measurements. Atmospheric Environment, 165, 23–34.
589 https://doi.org/10.1016/j.atmosenv.2017.06.027
590
591 King, M. D., Canosa-Mas, C. E. and Wayne R. P. (2001). Gas-phase reactions between RO_2 and
592 NO, HO_2 or CH_3O_2: correlations between rate constants and the SOMO energy of the peroxy (RO_2)
593 radical. Atmospheric Environment 35.12 (2001): 2081-2088. https://doi.org/10.1016/S1352-
594 2310(00)00501-X
595
596 Knote, C., Tuccella, P., Curci, G., Emmons, L., Orlando, J. J. Madronich, S., Baró, R., Jiménez-
597 Guerrero, P., Luecken, D., Hogrefe, C., Forkel, R., Werhahn, J., Hirtl, M., Pérez, J. L., San José,
598 R., Giordano, L., Brunner, D., Yahya, K., Zhang, Y., Influence of the choice of gas-phase
599 mechanism on predictions of key gaseous pollutants during the AQMEII phase-2 intercomparison.
600 Atmospheric Environment 115 (2015): 553-568. https://doi.org/10.1016/j.atmosenv.2014.11.066.
601
602 Li, J. (2019). Quantifying the nitrogen equilibrium and photochemistry-induced kinetic isotopic
603 effects between NO and NO_2. Retrieved from osf.io/jw8hu
604
605 Madronich, S., & Flocke, S. (1999). The role of solar radiation in atmospheric chemistry. In
606 Environmental photochemistry (pp. 1–26). The Handbook of Environmental Chemistry (Reactions
607 and Processes), vol 2 / 2L. Springer, Berlin, Heidelberg. https://doi.org/10.1007/978-3-540-69044-
608 3_1
609
610 Mazzeo, N. A., Venegas, L. E., & Choren, H. (2005). Analysis of NO, NO_2, O_3 and NO_x
611 concentrations measured at a green area of Buenos Aires City during wintertime. Atmospheric
612 Environment, 39(17), 3055–3068. https://doi.org/10.1016/j.atmosenv.2005.01.029
613
614 McIlvin, M. R., & Altabet, M. A. (2005). Chemical conversion of nitrate and nitrite to nitrous
615 oxide for nitrogen and oxygen isotopic analysis in freshwater and seawater. Analytical Chemistry,
616 77(17), 5589–5595. https://doi.org/10.1021/ac050528s
617
618 Michalski, G., Jost, R., Sugny, D., Joyeux, M., & Thiemens, M. (2004). Dissociation energies of
619 six NO_2 isotopologues by laser induced fluorescence spectroscopy and zero-point energy of some
620 triatomic molecules. The Journal of Chemical Physics, 121(15), 7153–7161.
621 https://doi.org/10.1063/1.1792233
622
623 Michalski, G., Bockheim, J. G., Kendall, C., & Thiemens, M. (2005). Isotopic composition of
624 Antarctic Dry Valley nitrate: Implications for NO_y sources and cycling in Antarctica. Geophysical
625 Research Letters, 32(13). https://doi.org/10.1029/2004GL022121
626

627 Miller, C. E., & Yung, Y. L. (2000). Photo-induced isotopic fractionation. Journal of Geophysical
628 Research: Atmospheres, 105(D23), 29039–29051. https://doi.org/10.1029/2000JD900388
629
630 Monse, E. U., Spindel, W., & Stern, M. J. (1969). Analysis of isotope-effect calculations illustrated
631 with exchange equilibria among oxynitrogen compounds. Rutgers-The State Univ., Newark, NJ.
632 DOI: 10.1021/ba-1969-0089.ch009
633
634 Morin, S., Savarino, J., Frey, M. M., Domine, F., Jacobi, H.-W., Kaleschke, L., & Martins, J. M.
635 F. (2009). Comprehensive isotopic composition of atmospheric nitrate in the Atlantic Ocean
636 boundary layer from 65°S to 79°N. J. Geophys. Res, 114. https://doi.org/10.1029/2008JD010696
637
638 Park, Y.-M., Park, K.-S., Kim, H., Yu, S.-M., Noh, S., Kim, M.-S., Kim, J.-Y., Ahn, J.-Y., Lee,
639 M.-D., Seok, K.-S., Kin, Y.-H., (2018). Characterizing isotopic compositions of TC-C, NO_3^--N,
640 and NH_4^+-N in PM2.5 in South Korea: Impact of China's winter heating.
641 https://doi.org/10.1016/j.envpol.2017.10.072
642
643 Saliba, N. A., Yang, H., & Finlayson-Pitts, B. J. (2001). Reaction of gaseous nitric oxide with
644 nitric acid on silica surfaces in the presence of water at room temperature. The Journal of Physical
645 Chemistry A, 105(45), 10339–10346. https://doi.org/10.1021/jp012330r
646
647 Savarino, J., Morin, S., Erbland, J., Grannec, F., Patey, M. D., Vicars, W., Alexander, B.,
648 Achterberg, E. P., (2013). Isotopic composition of atmospheric nitrate in a tropical marine
649 boundary layer. Proceedings of the National Academy of Sciences, 110(44), 17668–17673.
650 https://doi.org/10.1073/pnas.1216639110
651
652 Sharma, H. D., Jervis, R. E., & Wong, K. Y. (1970). Isotopic exchange reactions in nitrogen oxides.
653 The Journal of Physical Chemistry, 74(4), 923–933. https://doi.org/10.1021/j100699a044
654
655 Takei, T., Yamazaki, A., Watanabe, T., & Chikazawa, M. (1997). Water adsorption properties on
656 porous silica glass surface modified by trimethylsilyl groups. Journal of Colloid and Interface
657 Science, 188(2), 409–414. https://doi.org/10.1006/jcis.1997.4777
658
659 Urey, H. C. (1947). The thermodynamic properties of isotopic substances. Journal of the Chemical
660 Society (Resumed), 562-581. https://doi.org/10.1039/JR9470000562
661
662 Vicars, W. C., Morin, S., Savarino, J., Wagner, N. L., Erbland, J., Vince, E., Martins, J. M. F.,
663 Lerner, B. M., Quinn, P. K., Coffman, D. J., Williams, E. J., Brown, S. S., (2013). Spatial and
664 diurnal variability in reactive nitrogen oxide chemistry as reflected in the isotopic composition of
665 atmospheric nitrate: Results from the CalNex 2010 field study. Journal of Geophysical Research:
666 Atmospheres, 118(18), 10–567. https://doi.org/10.1002/jgrd.50680
667
668 Walters, W. W., & Michalski, G. (2015). Theoretical calculation of nitrogen isotope equilibrium
669 exchange fractionation factors for various NO_y molecules. Geochimica et Cosmochimica Acta,
670 164, 284–297. https://doi.org/10.1016/j.gca.2015.05.029
671

Walters, W. W., Goodwin, S. R., & Michalski, G. (2015). Nitrogen stable isotope composition ($\delta^{15}N$) of vehicle-emitted NO_x. Environmental Science & Technology, 49(4), 2278–2285. https://doi.org/10.1021/es505580v

Walters, W. W., & Michalski, G. (2016). Ab initio study of nitrogen and position-specific oxygen kinetic isotope effects in the $NO+O_3$ reaction. The Journal of chemical physics, 145(22), 224311. https://doi.org/10.1063/1.4968562

Walters, W. W., Simonini, D. S., & Michalski, G. (2016). Nitrogen isotope exchange between NO and NO_2 and its implications for $\delta^{15}N$ variations in tropospheric NO_x and atmospheric nitrate. Geophysical Research Letters, 43(1), 440–448. https://doi.org/10.1002/2015GL066438

Walters, W. W., Fang, H., & Michalski, G. (2018). Summertime diurnal variations in the isotopic composition of atmospheric nitrogen dioxide at a small midwestern United States city. Atmospheric Environment, 179, 1–11. https://doi.org/10.1016/j.atmosenv.2018.01.047

Williams, E. L., & Grosjean, D. (1990). Removal of atmospheric oxidants with annular denuders. Environmental Science & Technology, 24(6), 811–814. https://doi.org/10.1021/es00076a002

Yang, J., Honrath, R. E., Peterson, M. C., Dibb, J. E., Sumner, A. L., Shepson, P. B., Frey, M., Jacobi, H.-W., Swanson, A., Blake, N., (2002). Impacts of snowpack emissions on deduced levels of OH and peroxy radicals at Summit, Greenland. Atmospheric Environment, 36(15–16), 2523–2534. https://doi.org/10.1016/S1352-2310(02)00128-0

Zhang, X., Ortega, J., Huang, Y., Shertz, S., Tyndall, G. S., & Orlando, J. J. (2018). A steady-state continuous flow chamber for the study of daytime and nighttime chemistry under atmospherically relevant NO levels. Atmospheric Measurement Techniques, 11(5), 2537–2551. https://doi.org/10.5194/amt-11-2537-2018

Zong, Z., Wang, X., Tian, C., Chen, Y., Fang, Y., Zhang, F., Li, C., Sun, J., Li, J., Zhang, G., (2017). First assessment of NO_x sources at a regional background site in North China using isotopic analysis linked with modeling. Environmental Science & Technology, 51(11), 5923–5931. https://doi.org/10.1021/acs.est.6b06316

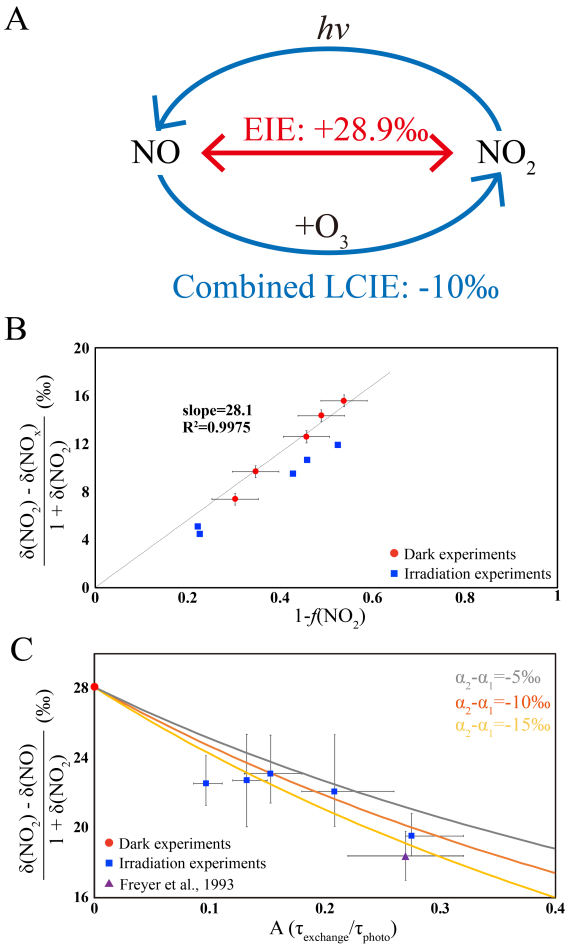

Fig. 1 A. a sketch of the isotopic fractionation processes between NO and NO_2, both fractionation factors are determined in this work. **B.** Results from five dark experiments (red circles) yielded a line with slope of 28.1‰ and an α(NO_2-NO) value of 1.0289, while the results from five UV irradiation experiments (blue squares) showed a smaller slope; **C.** Results from five UV irradiation experiments (blue squares) and a previous field study (purple triangle), comparing to the dark experiments (red circle). The three lines represent different (α_2-α_1) values: the (α_2-α_1) = -10 ‰ line showed the lowest RMSE to our experimental data as well as the previous field observations. The error bars in panels B and C represented the combined uncertainties of NO_x concentration measurements and isotopic analysis.

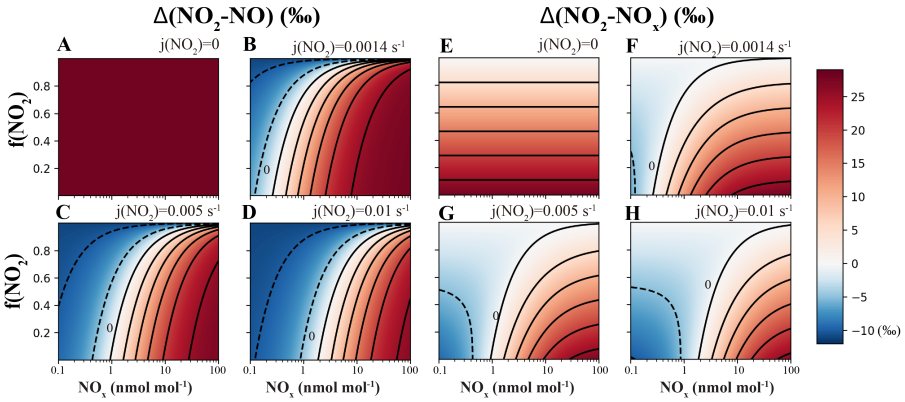

Fig. 2 Calculating isotopic fractionation values between NO-NO_2 ($\Delta(NO_2\text{-}NO)$, **A-D**) and NO_x-NO_2 ($\Delta(NO_2\text{-}NO_x)$, **E-H**) at various $j(NO_2)$, NO_x level and $f(NO_2)$ using Eq. (7) and (8). Each panel represents a fixed $j(NO_2)$ value (showing on the upper right side of each panel), and the fractionation values are shown by color. Lines are contours with the same fractionation values, at an interval of 5‰, the contour line representing 0‰ was marked on each panel except for A and E.

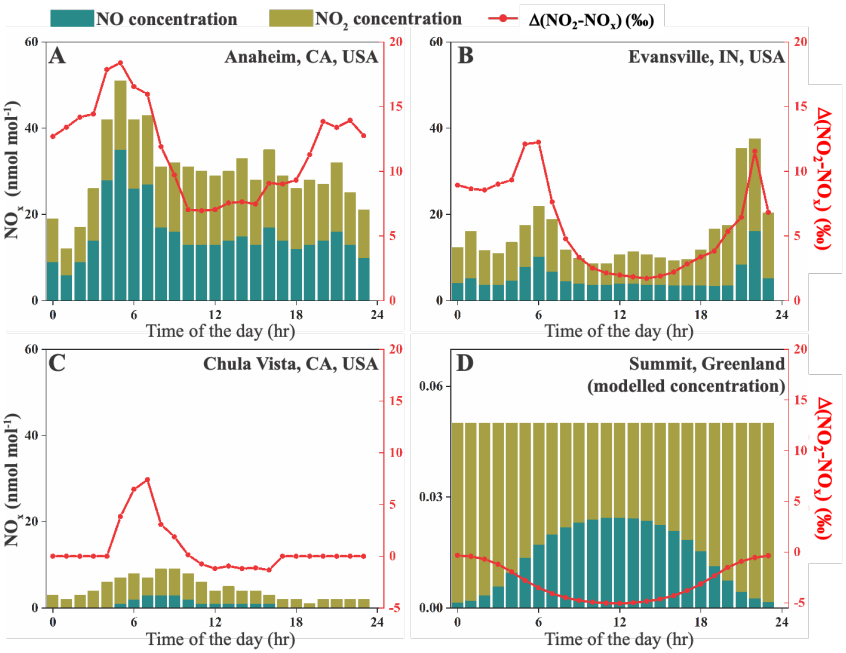

Fig. 3 NO_x concentrations and calculated $\Delta(NO_2\text{-}NO_x)$ values at four sites. Stacked bars show the NO and NO_2 concentrations extracted from monitoring sites (A-C) or calculated using 0-D box model (D); the red lines are $\Delta(NO_2\text{-}NO_x)$ values at each site. Note that the NO_x concentration (left-y) axis on panel D is different from the rest.

Experiment	Number	NO conc. (nmol mol^{-1})	NO_2 conc. (nmol mol^{-1})	O_3 conc. (nmol mol^{-1})	$\delta(NO_2)$ (‰)	$f(NO_2)$
Determining $\delta(NO_x)$	1	0.0	17.8	13.4	-59.5	1.00
	2	0.0	61.3	0.5	-58.9	1.00
	3	0.0	18.9	10.7	-58.0	1.00
Dark experiments	1	16.0	36.8	0.0	-51.8	0.70
	2	33.6	28.8	0.0	-43.9	0.46
	3	6.7	12.6	0.0	-49.6	0.65
	4	16.2	16.9	0.0	-45.1	0.51
	5	20.4	24.2	0.0	-46.8	0.54
Irradiation experiments	1	7.1	6.4	2.8	-47.5	0.47
	2	4.5	5.3	4.5	-48.7	0.54
	3	3.3	4.4	4.2	-49.8	0.57
	4	2.5	8.5	10.7	-54.6	0.77
	5	5.2	18.1	11.0	-54.0	0.78

Table 1. Experimental conditions, concentrations of NO, NO_2 and O_3 at steady state, and measured $\delta(NO_2)$ values.

Deleted: ppb

Deleted: ppb

Deleted: ppb

Appendix A. Chamber descriptions

The chamber is a 10 m^3 Teflon bag equipped with several standard instruments including temperature and humidity probe, NO_x monitor and O_3 monitor. 128 wall-mounted blacklight tubes surrounded the chamber to mimic tropospheric photochemistry and the photolysis rate of NO_2 ($j(NO_2)$) when all lights are on have been previously determined to be 1.4×10^{-3} s^{-1}, similar to a $j(NO_2)$ coefficient at an 81-degree solar zenith angle. The irradiation spectrum of the blacklights are shown in Figure A1. The chamber was kept at room temperature and one atmospheric pressure. Before each experiment, the chamber was flushed with zero air at 40 L min^{-1} for at least 12 hours to ensure the background NO_x, O_3 and other trace gases were below detection limit.

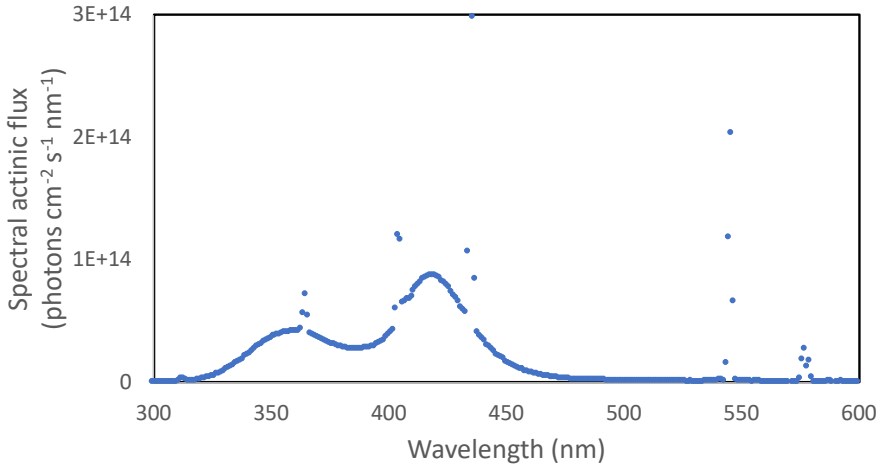

Figure A1 Spectral actinic flux versus wavelengths of the UV light source used in our experiments.

748 **Appendix B. Box model assessing the time needed for NO-NO_2 to reach isotopic equilibrium**

749 The time needed to reach NO-NO_2 isotopic equilibrium during light-off experiments were
750 assessed using a 0-D box model. This box model contains only two reactions:

751 $^{15}NO_2 + {}^{14}NO \rightarrow {}^{15}NO + {}^{14}NO_2$ $k = 8.14000 \times 10^{-14}$ cm^3 s^{-1}

752 $^{15}NO + {}^{14}NO_2 \rightarrow {}^{15}NO_2 + {}^{14}NO$ $k' = 8.37525 \times 10^{-14}$ cm^3 s^{-1}

753 Where k and k' are rate constants of the reactions. The differences in rate constants were calculated
754 by assuming an $\alpha(NO_2\text{-}NO)$ value of 1.0289. Six simulations were conducted at various initial NO
755 (with $\delta^{15}N = 0‰$) and O_3 levels that were similar to our experiment. Then the $\delta^{15}N$ values of NO
756 and NO_2 during the simulation were calculated from the model and were shown in Figure B1,
757 suggesting that in our experimental condition, all systems should reach isotopic equilibrium within
758 1 hr.

759

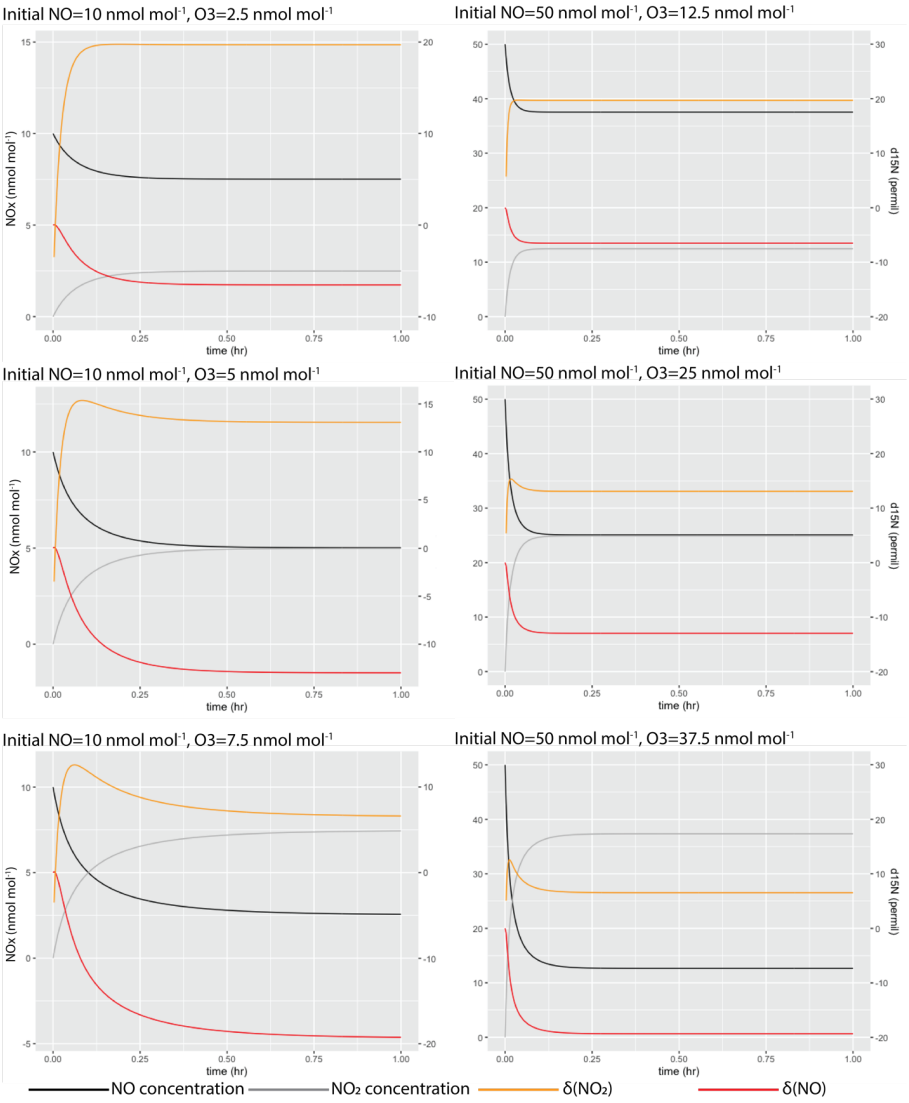

760

761 Figure B1 Simulated NO-NO_2 isotopic equilibrium process in the chamber at various NO and O_3

762 concentrations.

Appendix C. Deriving Equations 7 and 8

When the system (R1-R6) reaches steady-state, we have:

$$d[^{15}NO_2]/dt=0 \quad \text{Eq. (C1)}$$

Therefore, using R1-R6:

$$k_1\,[^{15}NO_2][^{14}NO]+j(NO_2)\alpha_1[^{15}NO_2]=$$

$$k_5\alpha_2[^{15}NO][O_3]+ k_1\alpha(NO_2\text{-}NO)\,[^{15}NO][^{14}NO_2] \quad \text{Eq. (C2)}$$

From here we refer $^{14}NO_2$ and ^{14}NO as NO_2 and NO for convenience, rearrange the above equation, we get:

$$\frac{[^{15}NO_2]}{[^{15}NO]} = \frac{k_5\alpha_2[O_3]+k_1\alpha(NO_2-NO)\,[NO_2]}{j_{NO2}\alpha_1+k_1[NO]} \quad \text{Eq. (C3)}$$

Meantime, since the Leighton cycle reaction still holds for the majority isotopes (NO and NO_2), we have:

$$j_{NO2}[NO_2]= k_5[NO][O_3] \quad \text{Eq. (C4)}$$

Thus,

$$\frac{[NO_2]}{[NO]} = \frac{k_5\times[O_3]}{j_{NO2}} \quad \text{Eq. (C5)}$$

From the text, when $j_{NO2}>0$, we defined $A=\tau_{exchange}/\tau_{photo}=j_{NO2}/(k_1\times[NO])$. Using the above equations, we know:

$$\frac{j_{NO2}}{[NO]} = \frac{k_5[O_3]}{[NO_2]} = Ak_1 \quad \text{Eq. (C6)}$$

$$\frac{j_{NO2}}{k_1[NO]} = \frac{k_5[O_3]}{k_1[NO_2]} = A \quad \text{Eq. (C7)}$$

Next, to calculate $\delta(NO_2)$-$\delta(NO)$, we use the definition of delta notation:

$$\delta(NO_2)\text{-}\delta(NO) = R_{NO2}/R_{std}\text{-}\ R_{NO}/R_{std} = (R_{NO2}/R_{NO}\text{-}1)(1+\delta(NO)) \quad \text{Eq. (C8)}$$

784 $$\frac{R_{NO2}}{R_{NO}} = \frac{[^{15}NO_2][NO]}{[^{15}NO][NO_2]} = \frac{k_5\alpha_2[O_3][NO]+k_1\alpha(NO_2-NO)[NO_2][NO]}{j_{NO2}\alpha_1[NO_2]+k_1[NO][NO_2]}$$ Eq. (C9)

785 Divide both side by $k_1[NO][NO_2]$:

786 $$\frac{R_{NO2}}{R_{NO}} = \frac{\frac{k_5\alpha_2[O_3]}{k_1[NO_2]}+\alpha(NO_2-NO)}{\frac{j_{NO2}\alpha_1}{k_1[NO]}+1}$$ Eq. (C10)

787 Rearrange and substitute $\frac{k_5[O_3]}{k_1[NO_2]}$ and $\frac{j_{NO2}}{k_1[NO]}$ with A:

788 $$\frac{R_{NO2}}{R_{NO}} = \frac{\alpha_2 A+\alpha(NO_2-NO)}{\alpha_1 A+1}$$ Eq. (C11)

789 $$\frac{R_{NO}}{R_{NO2}} = \frac{\alpha_1 A+1}{\alpha_2 A+\alpha(NO_2-NO)}$$ Eq. (C12)

790 $$\frac{R_{NO}}{R_{NO2}} - 1 = \frac{(\alpha_1-\alpha_2)A-(\alpha(NO_2-NO)-1)}{\alpha_1 A+\alpha(NO_2-NO)}$$ Eq. (C13)

791 Thus,

792 $$\delta(NO_2)\text{-}\delta(NO)=\frac{(\alpha_2-\alpha_1)A+(\alpha(NO_2-NO)-1)}{\alpha_1 A+\alpha(NO_2-NO)}(1+\delta(NO_2))$$ Eq. (C14)

793 Then, using mass balance:

794 $$\delta(NO_2)\,f(NO_2)+\delta(NO)(1-f(NO_2)) = \delta(NO_x)$$ Eq. (C15)

795 We can derive Eq. 8:

796 $$\delta(NO_2)\text{-}\delta(NO_x)=\frac{(\alpha_2-\alpha_1)\times A+\alpha(NO_2-NO)-1)}{\alpha_1 A+\alpha(NO_2-NO)}\,(1+\delta(NO_2))\,(1-f(NO_2))$$ Eq. (C16)